Journal of Environmental Chemical Engineering 7 (2019) 103461

Contents lists available at ScienceDirect

Journal of Environmental Chemical Engineering

journal homepage: www.elsevier.com/locate/jece

Synthesis of amine and thiol dual functionalized graphene oxide for aqueous sequestration of lead

Paul N. Diagboya[a,*], Herry K. Mmako[a], Ezekiel D. Dikio[b], Fanyana M. Mtunzi[a]

[a] Department of Chemistry, Vaal University of Technology, Vanderbijlpark, South Africa
[b] Department of Chemical Sciences, Niger Delta University, Wilberforce Island, Bayelsa State, Nigeria

ARTICLE INFO

Keywords:
Amine functionalized graphene oxide
Thiol functionalized graphene oxide
Amine and thiol functionalized graphene oxide
Water treatment
Adsorption

ABSTRACT

Recent advances in graphene chemistry indicate that it may play vital role in water treatment processes, especially when synergistically coupled with other functional moieties. Thus, graphene oxide (GO) was mono/dual-functionalized with amino and thiol groups to obtain amino–GO (GONH), thiol–GO (GOSH) and amino/thiol–GO (GOSN). These were characterized and used for Pb(II) adsorption. The Fourier transform infrared spectroscopy (FTIR), X-ray diffraction and thermogravimetric analysis confirmed the success of these syntheses. The adsorption process was spontaneous and endothermic, while the rate was high with up to 80% of total adsorption occurring within the initial 30 min of starting the experiment. Adsorption mechanism involved electrostatic interactions between active functional groups and the Pb(II) cations, but the data fits to models (either Langmuir, Freundlich or Brouers–Sotolongo–fractal adsorption isotherm model) were dependent on the specific functional groups involved on the adsorbent involved in the process. For instance, adsorption on the highly electrostatic functional groups having oxygen and nitrogen followed Langmuir model, while a combination of the weak and strong functional groups (involving the above as well as sulphur groups) followed the Freundlich or the more complex Brouers–Sotolongo–fractal adsorption isotherm model. The adsorption capacity of GONH (138.0 mg/g) was higher than for the GOSH (101.5 mg/g) and GOSN (97.8 mg/g), but relative to other adsorbents reported in literature, these values point to their potential for treatment of Pb(II) in real wastewater.

1. Introduction

The extent of surface water contamination is enormous and the remediation is seemingly intractable due to the diverse nature of contaminants' sources [1]. From natural disasters/war-ravaged climes to stable ones, there is limited access to usable and hygienic fresh water, and reports show the situation is not ameliorating but growing worse yearly [2–6]. Hence, finding cost-effective technologies that can achieve easy, fast and high efficiency in water treatment is paramount.

The toxic metal Pb is particularly ubiquitous in water systems with low maximum contaminant level in drinking water of 15 μg/L, and causing neurological and reproductive health defects as well as hypertension [7]. Hence it will be used as a model pollutant in this study. Several adsorbents have been studied for water treatment purposes including adsorbents such as activated carbon [8], zeolite [9], biomasses [10,11], clays [11] and porous materials [1], as well as nanofiltration techniques [12,13]. However, the unfolding chemistry of porous materials in several recent studies indicates that porous materials may play vital roles in water treatment processes [14]. Typical examples of these materials include porous silica and graphene, as well as their functionalized derivatives [1,15]. Graphene, a single layer planar sheet consisting of sp^2 carbon atoms covalently bonded in honeycomb crystal lattice has attracted a great deal of attention due to its exceptional mechanical, electrical, thermal and optical properties, as well as its very high theoretical specific surface area (2630 m^2/g) and the ability to easily influence these properties through chemical functionalization [16]. Recent advances in the chemistry of graphene and its oxide have triggered enormous interests in adsorption science because virtually any desired functional group can be tailored into the graphene sheet to work in synergy [17,18]. Synergistic combination of different molecules to form a single product has become a very successful approach in materials science for achieving highly efficient and specific goals in the property of materials; thus making products with superior structural and functional properties to those of the individual pure components [3,17–21]; this may be important in improving current water treatment techniques.

To obtain efficient synergistic graphene materials, several chemical procedures have been employed and among them is functionalization of

* Corresponding author.
E-mail address: pauldn2@yahoo.com (P.N. Diagboya).

https://doi.org/10.1016/j.jece.2019.103461
Received 17 April 2019; Received in revised form 23 September 2019; Accepted 5 October 2019
Available online 11 October 2019
2213-3437/

pristine graphene and graphene oxide sheets with organic functional groups [17,22,23]. Functionalization includes the synergistic coupling, either by covalent or electrostatic interaction, of useful functional groups to the graphene and graphene oxide sheets. Covalent organic functionalization reactions of graphene might be either through the formation of bonds between free radicals or dienophiles and C=C bonds of pristine graphene, or the formation of bonds between organic functional groups and the oxygen groups of graphene oxide [3,17].

Usually, to remove contaminants from aqueous solution, graphene and graphene oxide have been functionalized with one major active group [18,20,24]. However, considering the theoretical surface area of graphene and the plethora of possible surface functional groups that can be added, coupling large quantities of useful and oppositely charged functional groups to the surface would result in an amphiphilic product containing several active functional centers for adsorption. This approach would almost certainly be useful for the simultaneous removal of both cationic and anionic contaminants from water. Hence, the aim of this study was to design, synthesize and compare single and dual-functionalized graphene oxide adsorbents using amine and thiol functional groups from (3-aminopropyl)-triethoxysilane and (3-mercaptopropyl)-triethoxysilane, respectively. The adsorbents were subsequently tested for the removal of Pb(II) from aqueous solutions while the adsorption data were described using various adsorption isotherm models.

2. Materials and methods

2.1. Synthesis and characterizations of amino/thiol-mono/dual-functionalized graphene oxide

All chemicals used for this study were of analytical grade and used without further treatment. They include graphite flakes from Sigma-Aldrich, while potassium permanganate, sulphuric acid, potassium dichromate and sodium nitrate were from Rochelle Chemicals, South Africa; hydrogen peroxide was from Merck, while (3-aminopropyl)-triethoxysilane (APTES) and (3-mercaptopropyl)-triethoxysilane (MPTES) were both from Acros Organics.

Graphene oxide (GO) was prepared by exfoliation of natural flake graphite using the modified Hummer's method [18]. Typically, natural flake graphite was oxidized in sodium nitrate and sulphuric acid on an ice water bath, followed by gradual addition of potassium permanganate, cooling, addition of 5% sulphuric acid and then hydrogen peroxide. The clean GO was obtained by a multi-cycle purification process and the concentration was determined thereafter.

Synthesis of the amino/thiol-mono-functionalized GO followed similar method [25]; the GO sheets were dispersed in 2% vol. APTES or MPTES in toluene, this was refluxed at 100 °C for 3 h, cooled to room temperature and the amino-functionalized GO (GONH) and thiol-functionalized GO (GOSH), respectively, were washed twice to remove any adsorbed reagents by dispersal in toluene while stirring for 20 min and sonicating for 5 min. The adsorbents were recovered by vacuum filtration and drying. Synthesis of the dual (amino and thiol) functionalized GO (GOSN) followed the same method expect that 2% vol. each of APTES and MPTES in the same toluene solution was used. The Fig. 1 shows the synthesis reaction scheme. The adsorbents (GO, GONH, GOSH and GOSN) were characterized using *Spectrum Two* Fourier transform infrared (FTIR) spectrometer (Perkin Elmer Instruments, USA), *Perkin- Elmer TGA 4000* Thermo-gravimetric analyzer (Perkin Elmer Instruments, USA), and X-ray diffractometer (XRD-7000, Shimadzu, Japan).

2.2. Adsorption studies

The GONH, GOSH and GOSN were used for Pb(II) adsorption experiments. The effects of the various operating variables were studied–time, pH, concentration and temperature. Typically, the adsorption experiments were carried out by weighing approximately 10.0 mg of the GONH, GOSH or GOSN into 50 mL plastic centrifuge bottles which were consequently added 20 mL Pb(II) solution of predetermined concentration. Where desired, the mixtures pH values were adjusted by either 0.1 M NaOH or HCl solution. The adsorbent and Pb(II) solution mixtures were incubated by shaking in an orbital shaker at 150 rpm until equilibrium. Subsequently, the adsorbent was separated from solution by centrifugation at 4000 rpm for 6 min and the quantity of Pb (II) ions left in solution determined by a Shimadzu AA-7000 (Japan) flame atomic absorption spectrophotometer (Supplementary information, SI 1). The studies time ran from 5 to 360 min (time), the pH from 3 to 6, concentration from 50 to 150 mg/L of Pb(II) and temperature from 16 to 37 °C. Apart from the effect of time, equilibrium time of 180 min was used, Pb(II) concentration of 100 mg/L (apart from effect of concentration), and all experiments were carried out in replicate.

2.3. Data treatment and management

The quantity of Pb(II) adsorbed per gram of adsorbent (q_e) was calculated from: $q_e = (C_O - C_e)V/m$; where the initial and final concentrations (mg/L) are C_o and C_e, while the adsorbent mass and solution volume are m (g) and V (mL), respectively. The rate data were described using the Lagergren [26] Pseudo-First Order (PFO) kinetic model [$q_t = q_e(1 - e^{-k_1 t})$] and Pseudo-Second Order (PSO) kinetic model [$q_t = (q_e^2 k_2 t)/(1 + q_e k_2 t)$]; where q_t (mg/g), k_1 (/min) and k_2 (g/g/min) are the adsorption at time t, the rate constants for PFO and PSO, respectively.

The equilibrium data were described using the Langmuir [27] [$q_e = (Q_O bC^e)/(1 + bC_e)$], Freundlich [28] [$q_e = k_f C_e^n$] and the Brouers–Sotolongo fractal [11] [$Q_e = Q_{max}(1 - (\exp(-K^w C_e^\alpha))$] adsorption isotherm models; where $Q_{o/max}$, b, k_f, n and α are the maximum adsorption capacity per unit weight, Langmuir energy-related parameter, Freundlich model adsorption constant, isotherm linearity parameter, and the fractional time index, respectively; while $K_w = k_f/Q_{max}$. The equations $LnK_o = (\Delta S^o/R) - (\Delta H^o/RT)$ and $\Delta G^o = -RTLnK_o$ were used to obtain the thermodynamic enthalpy change (ΔH^o), entropy change (ΔS^o) and Gibbs free energy (ΔG^o). All model fittings (SM Fig. 2) were carried out the nonlinear equations on the OriginPro 8 software.

3. Results and discussion

3.1. Physicochemical characterizations

Schematics of the synthesis of GONH, GOSH and GOSN adsorbents are depicted in Fig. 1. Typically, the GO was first dispersed in a 2% organosilane [(3-aminopropyl)-triethoxysilane and/or (3-mercaptopropyl)-triethoxysilane] toluene solution, and the solution was refluxed for 3 h. These organosilane moieties were covalently grafted onto the GO surface via reaction between the GO hydroxyl group and the less hydrolytically stable bond of the H_3C–O on the organosilane. The results of the physicochemical characterizations showed in Fig. 2*a–f* and 3*a–c* point to the successes of these syntheses. The Fourier transform infrared spectroscopy (FTIR) spectra (2*a*) revealed the presence of characteristic bands of the GO as well as bands which could be associated with the APTES and MPTES linkages in the new adsorbents. The intensity of wide band around 3340 cm^{-1} which corresponds to −OH functional group stretching vibrations on the GO sheets reduced in the APTES and MPTES mono-functionalized adsorbents (GONH and GOSH) but this band almost disappeared in the dual-functionalized adsorbent (GOSN). This is an indication that the APTES and MPTES groups were attached to the GO sheets via the −OH functional group positions, and with more of these modifying groups taking up the available −OH points (as in the case of the dual-functionalization) nearly all the −OH functional groups on the GO surface were used up resulting in the near disappearance of this band in the GOSN adsorbent. A new peak appeared in the adsorbents at ≈2930 cm^{-1}, and this has been attributed to

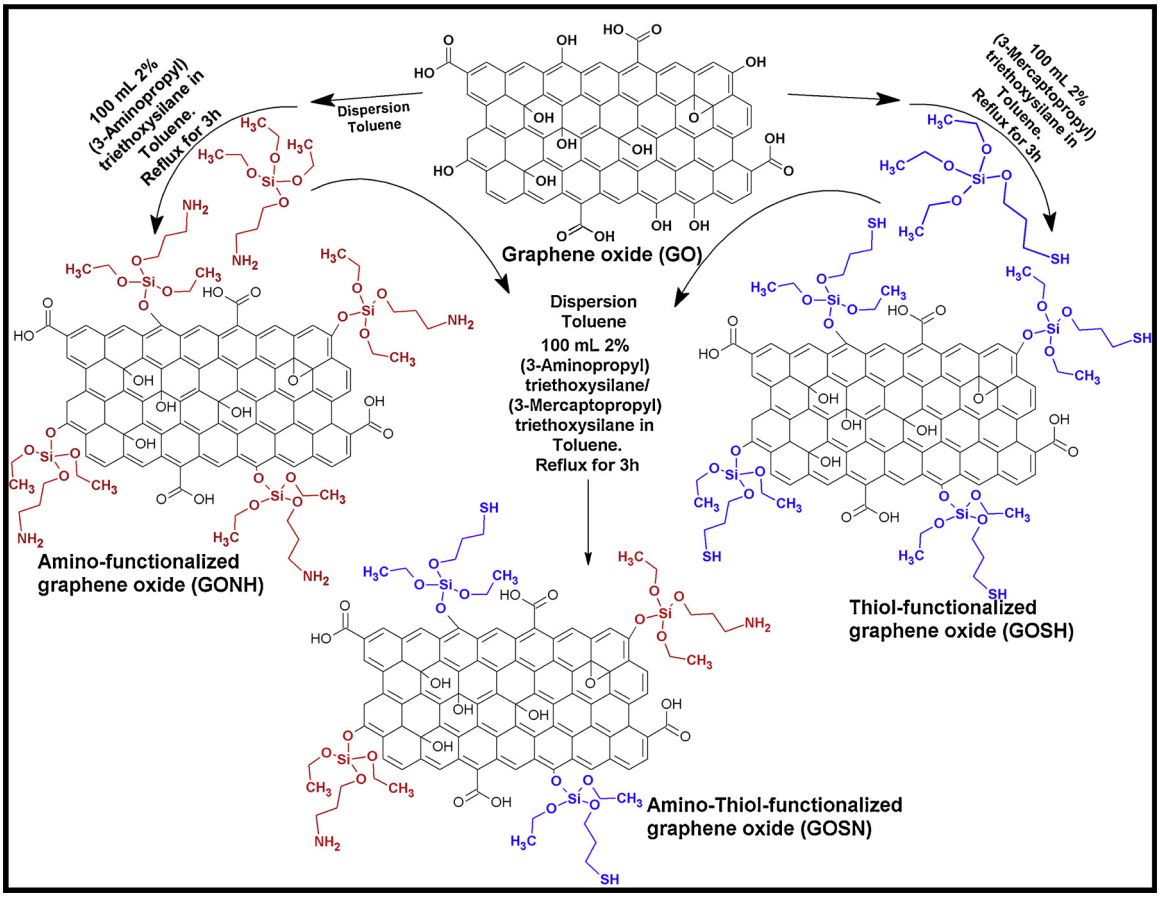

Fig. 1. Synthesis schematics for GONH, GOSH and GOSN.

vibrations from the CH_2—CH_2 group [25]. The GONH and GOSN peaks at 1649 cm^{-1} were attributed to amide I (C═O) and II (C—N) vibrations from the APTES moiety as well as the GO itself [3,25]; however, the lower intensity when compared with the pristine GO indicates that the functionalization has a shielding effect that reduces the effect of these groups in the final adsorbent. Similarly, this shielding effect was observed for the low intensity –SH group band at 2564 cm^{-1} in the pure MPTES spectra (Insert Fig. 2*a* (iv)) which was suppressed in the GOSH (with shift to ≈2545 cm^{-1}) and GOSN adsorbents. The prominent peaks around 1020 and 685 cm^{-1} were ascribed to the characteristic stretching vibrations of the silanol Si–O–Si group [25,29] and the out-of-plane C—H bending vibrations [30] from the APTES and MPTES moieties, respectively

The X-ray diffraction spectra (Fig. 2*b*) analysis revealed structural differences between the pristine GO and the functionalized adsorbents. The pristine GO (Fig. 2*b i*) exhibited an intense peak around $2\theta = 12^{\circ}$ with a broad but weak peak around 23°. These peaks are indications of the presence of polar oxygen containing functional groups formed during the graphite exfoliation [3,25]. In the XRD spectra patterns of the functionalized GO adsorbents (Fig. 2*b ii–iv*) the GO intense peak around $2\theta = 12^{\circ}$ became suppressed but the GO weak peak around $2\theta = 23^{\circ}$ became intense. The suppression of the intense peak around $2\theta = 12^{\circ}$ suggested a reduction in the amount of freely bonded hydroxyl groups in the new GO materials because the incoming moieties were attached via that point [31]. Comparing these peaks of the pristine and functionalized GO suggested reduced orderliness of the functionalized adsorbents [32] as the − OH functional groups were used up.

The TGA and DTA spectra of the adsorbents in the temperature range of 40–800 °C are shown in Fig. 2*c–f*. The Fig. 2*c* shows a comparative TGA for all adsorbents; it revealed that within this temperature range, GO lost over 70% of it mass while the functionalized GO adsorbents exhibited less losses (≈40%). This is another clear indication of the success of the synthesis technique and suggested that the functionalization increased the density per unit weight of the functionalized GO adsorbents. The TGA and DTA spectra of all three adsorbents (Fig. 2*d–f*) exhibited four major thermal transitions at approximately 110, 170, 330 and 520 °C. These thermal transitions maybe attributed to loss of physisorbed water molecules, decomposition of the labile oxygen/sulphur-containing surface functional groups (such as —CO, —COOH, —OH and –SH), as well as the partial breakdown of the APTES/MPTES structures and the GO backbone, respectively.

3.2. Adsorption kinetics

The GONH, GOSH and GOSN rate trends of Pb(II) adsorption are shown in Fig. 3*a* and the PFO and PSO kinetic models parameters in Table 1. The Fig. 3*a* revealed fast adsorption rates within the initial 30 min of starting the experiment with approximately 60–80% of the adsorption occurring here (stage *i*). This first adsorption stage or stage *i* was attributed to the fast Pb(II) cations adsorption on the abundant vacant adsorption sites at the beginning of the process. Beyond this stage, the rate slowed with approximately 20–40% of the adsorption occurring (stage *ii*). Equilibrium, which results in almost stable adsorption-desorption rates, was achieved at stage *ii* at 120 min but subsequent adsorption experiments (pH and equilibrium) were carried out at 180 min to give allowance for maximum adsorption. This later adsorption stage or stage *ii* was ascribed to slower adsorption rates close to equilibrium when fewer vacant adsorption sites are available both on the external surfaces as well as within the pores.

In order to predict the kinetics of the adsorption process, the rates data were fitted to and described using kinetic models in Table 1. A comparison of the nonlinear fittings of the PFO and PSO kinetic models

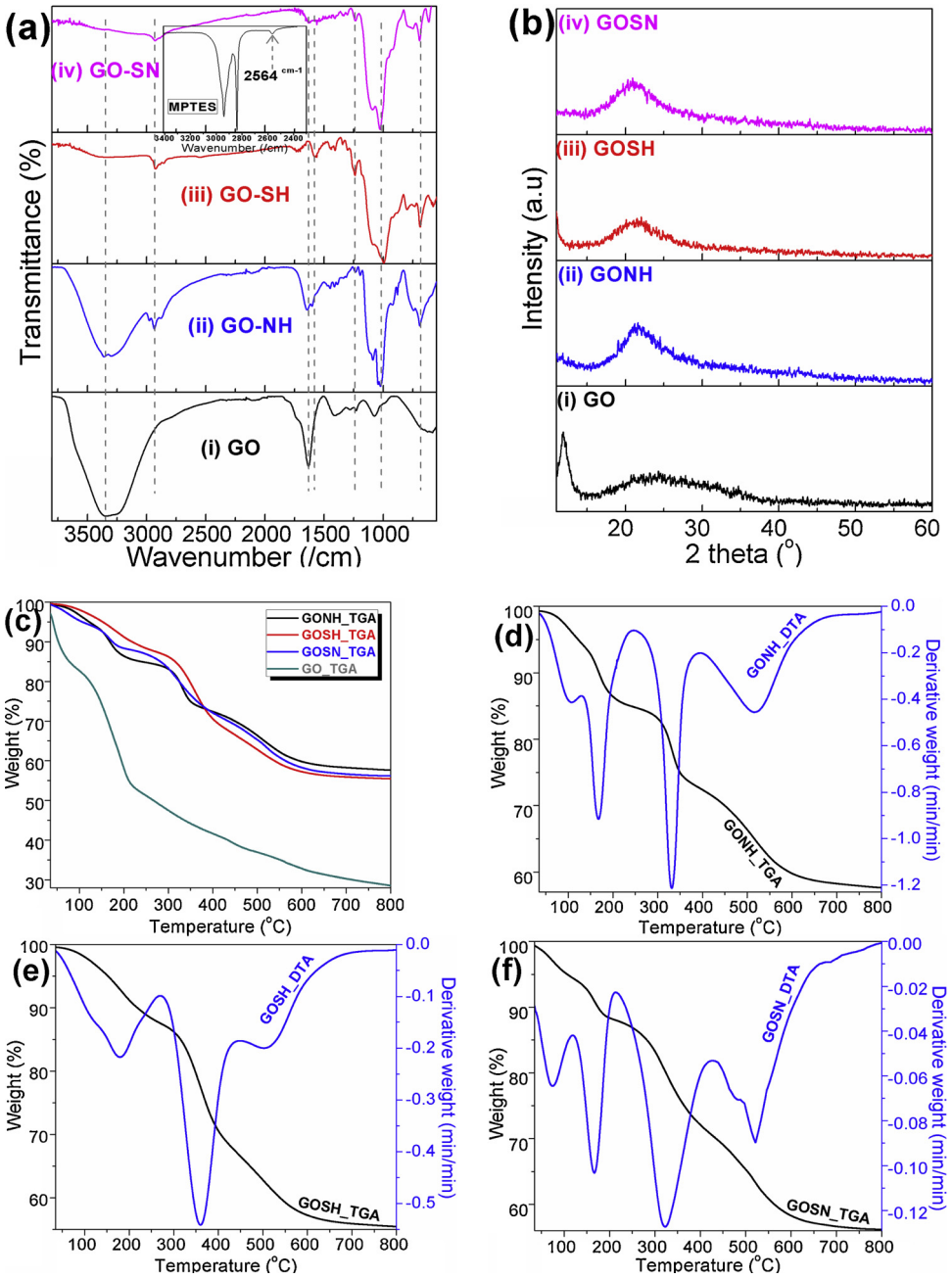

Fig. 2. (a) FTIR and (b) XRD spectra of (i) GO, (ii) GONH, (iii) GOSH, and (iv) GOSN; (c) TGA spectra of all adsorbents; TGA/DTA spectra of (d) GONH, (e) GOSH, and (f) GOSN.

with the experimental data was done using the correlation coefficients (r^2) and the equilibrium adsorption (q_e) values. The r^2 values of the PSO kinetic model was closer to unity and thus better correlated to experimental data than the PFO kinetic model, while the model also predicted the experimental q_e better. The good fit of the experimental data to the PSO kinetic model suggested that the mechanism of the adsorption process was mainly electrostatic interactions between active functional groups on these adsorbents and the aqueous Pb(II) cations [33]. Further insights into the adsorption mechanism would be obtained below from the adsorption isotherm models.

3.3. Effect of pH on Pb(II) adsorption

Solution pH affects the charge density on the adsorbate as well as the adsorbent; and consequently controls the extent of adsorption [34]. Thus, the effect of pH on Pb(II) adsorption trends on the GONH, GOSH and GOSN adsorbent were studied and the trends are depicted in Fig. 3*b*. The Fig. 3*b* revealed increased Pb(II) adsorption trends on these adsorbents as the solution pH rose from 3 to 6 and the optimum pH was observed between 5 and 6. This trend was mainly attributed to the charge density on the adsorbent at various pH values. At pH of 3, the concentration of protons in solution is very high and this effectively competes with the Pb(II) cations for the adsorption sites, as well as protonates several functional groups, including the hydroxyl, carbonates and amines. This results in uncharged adsorption sites with far reduced electrostatic attraction and consequently the observed low Pb (II) adsorption values. Conversely, as pH increased gradually, the quantity of protons and the competition for adsorption sites reduced accordingly, with a consequent increase in electrostatic attraction and the Pb(II) adsorption values.

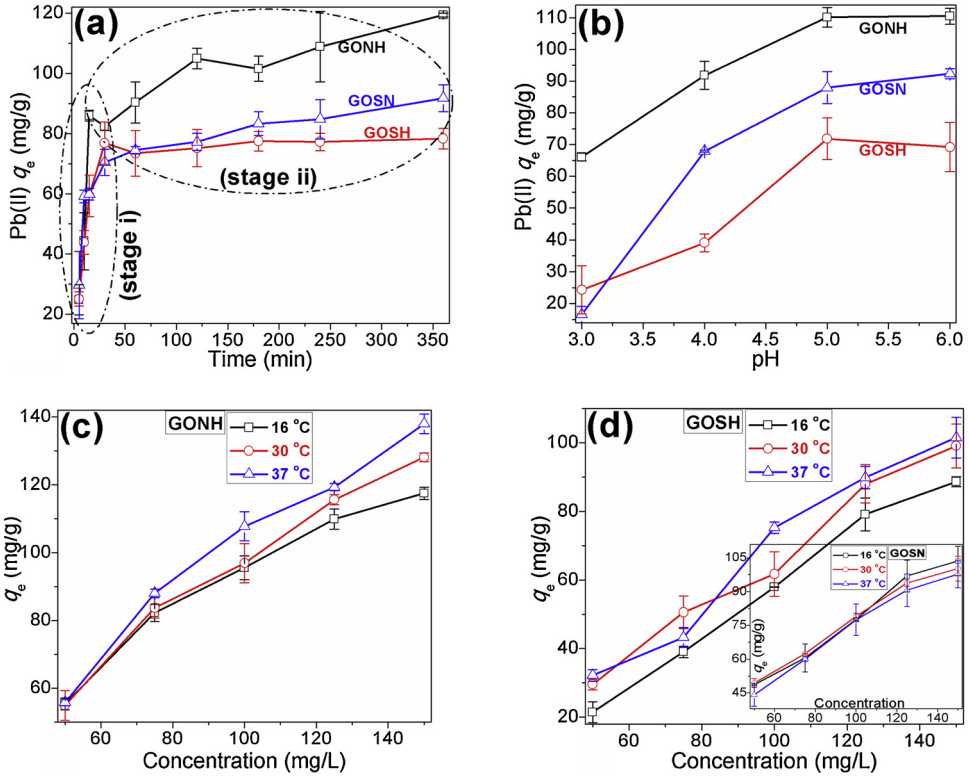

Fig. 3. The Pb(II) adsorption trends for GONH, GOSH and GOSN at varied (a) time and (b) pH; adsorption trends at varied Pb(II) concentrations and temperatures for (c) GONH, (d) GOSH (Insert: GOSN).

Table 1
Kinetic model parameters for Pb(II) adsorption on GONH, GOSH and GOSN.

Kinetic model	Parameter	GONH	GOSH	GOSN
*PFO	q_e (mg/g)	56.5	17.5	36.4
	k_1 (/min)	0.008	0.014	0.008
	r^2	0.7674	0.6083	0.8531
*PSO	q_e (mg/g)	120.7	79.7	91.8
	k_2 (g/mg/min)	0.0005	0.002	0.001
	r^2	0.9941	0.9994	0.9962
Experimental q_e	mg/g	119.4	78.3	91.7

* Pseudo-first order (PFO) model; *Pseudo-second order (PSO) model.

Table 2
Adsorption isotherm models parameters for Pb(II) adsorption.

Adsorption isotherm model	Parameter	GONH	GOSH	GOSN
Langmuir	Q_o (mg/g)	133.7	68.4	142.9
	β	1.99	0.002	0.069
	r^2	0.9212	0.0134	0.9751
Freundlich	n	83.4	3.2	20.8
	k_f	0.17	0.957	0.43
	r^2	0.8291	0.7784	0.9593
Brouers–Sotolongo–fractal	Q_{max}	125.1	569.3	102.5
	k_w	1.41	0.005	0.077
	α	1.0	1.0	1.0
	r^2	0.8982	0.7801	0.9490
Experimental q_e (mg/g)		138.0	101.5	97.8

3.4. Equilibrium adsorption of Pb(II) cations and effect of temperature

Equilibrium Pb(II) adsorption trends shown in Fig. 3*c–d* revealed increases in Pb(II) adsorption by all three adsorbents as concentration increased from 50 through 150 mg/L. Similar trends were also observed at the various temperatures studied: 16, 30 and 37 °C (Fig. 3*c–d*). Kabiri et al. [35] and Mohubedu et al. [33] have reported identical trends in literature. Diagboya and Dikio [34] have ascribed this trend to the behaviour of the adsorptives (Pb(II)), between the adsorbents surface adsorption sites and the internal ones. For a low adsorptive concentration at equilibrium, the movement of the adsorptives between the adsorbents surface and internal adsorption sites will be equal, and further movements will be significantly impermissible. Conversely, increasing the adsorptive concentration will re-initiate movement across these boundaries and hence the observed higher adsorption.

Further insight into the adsorption mechanism was obtained by fitting and describing equilibrium data using three adsorption isotherm models: the Langmuir, Freundlich and Brouers–Sotolongo fractal adsorption isotherm models. Comparison of these model parameters, as shown in Table 2, revealed that the GONH, GOSH and GOSN experimental data best fitted the Langmuir, Freundlich and Brouers–Sotolongo–fractal adsorption isotherm models, respectively. The best fits were measured by the closeness of the correlation coefficient (r^2) to unity, as well as the correlation of the experimental adsorption capacity ($Q_{o/max}$) to the model q_e values.

The good fits of the three adsorbents to dissimilar adsorption isotherm models may be related to the interaction between the main functional groups on the adsorption sites present on each adsorbent and the Pb(II) cations. For instance, the best fit of the GONH data to the Langmuir suggest that Pb(II) adsorption occurred on adsorption sites of equal energy for the Pb(II) ions (mainly the attached –NH groups) and only a monolayer of Pb(II) cations was formed at equilibrium [36,37]; the data also indicated strong affinity between Pb(II) and the –NH group. In contrast, the affinity was weaker for Pb(II) and the –SH group on the GOSH adsorbent, and the experimental data gave the best fit for the Freundlich adsorption isotherm model. This indicates Pb(II) adsorption on dissimilar sites of unequal energies (the attached –SH and possibly other groups such as −COO– with stronger affinity for Pb(II)) and possibly formation of multilayer of Pb(II) cations at equilibrium [38]. On the other hand, the best fit of the GOSN experimental data to the Brouers–Sotolongo–fractal adsorption isotherm model implied Pb

Table 3
Pb(II) adsorption on GONH, GOSH and GOSN thermodynamic parameters.

Thermodynamic Parameter		GONH	GOSH	GOSN
ΔH°	kJ mol^{-1}	22.86	23.77	8.13
ΔS°	J mol^{-1} K^{-1}	125.96	82.75	5.17
ΔG° (kJ mol^{-1})	289 K	–12.59	–0.09	–6.32
	303 K	–18.42	–1.49	–6.94
	310 K	–14.00	–1.75	–5.99

Table 4
Comparison of GONH, GOSH and GOSN Pb(II) adsorption capacities with other adsorbents in literature.

Adsorbent	q_e (mg/g)	Reported optimum conditions	Reference
Graphene nanosheets	35.5	Time: ≈10 min; pH: 7	[41]
Magnetic chitosan/graphene oxide	76.9	Time: 10 min; pH: 5	[42]
Graphene aerogels	80.0	Time: ≈100 min; pH: not available	[43]
GOSN	97.8	Time: 60 min; pH: 5	This study
Graphene oxide/chitosan composite	99.0	Time and pH data not available	[44]
GOSH	101.5	Time: 60 min; pH: 5	This study
SiO_2/graphene composite	113.6	Time: 20 min; pH: 6	[45]
GONH	138.0	Time: 120 min; pH: 5	This study
GO–SBA-15	255.1	Time: 10 min; pH: 5	[31]
$CoFe_2O_4$-rGO	299.4	Time: 10 min; pH: 5.3	[46]
Magnetic-EDTA-GO	508.4	Time: 40 min; pH: 4 to 5	[47]

(II) adsorption on heterogeneous adsorption sites with a more complex mechanism [11,39]. Thus, adsorption mechanism on the GOSN involved adsorption on the attached —NH, –SH and —COO– groups, and possibly complex Pb(II) co-ordination reactions involving the oxygen and nitrogen containing functional groups on the GOSN.

In order to ascertain the effect of temperature on Pb(II) adsorption thermodynamics by these adsorbents, the equilibrium data obtained at the various temperatures were evaluated using the thermodynamic parameters (ΔH°, ΔS° and ΔG°) whose values are shown in Table 3. The ΔG° values in Table 3 suggested that Pb(II) adsorption by the adsorbents at all temperatures studied were negative, and implied spontaneous and feasible processes. The ΔS° values were positive, and suggestive of increased randomness of the Pb(II) cations in solution as the processes proceeded towards equilibrium. The positive ΔH° values of these adsorbents indicate endothermic adsorption processes; thus, increase in temperature would result in increased Pb(II) adsorption as observed [40].

3.5. Comparison of adsorption capacities and FTIR spectra of pristine and Pb(II)–loaded adsorbents

The GONH, GOSH and GOSN Pb(II) adsorption capacities have been compared with some GO-based adsorbents recorded in literature (Table 4). The tabulated adsorption capacities showed that the three adsorbents performed higher than several recorded GO-based adsorbents which have been used for Pb(II) adsorption; but there were other adsorbents which performed better than our current adsorbents. Relative to these literature recorded adsorbents, the comparable adsorption capacities of our adsorbents points to the potential of these GO-based adsorbents for treatment of Pb(II) in real wastewater.

The FTIR spectra of the pristine GONH, GOSH and GOSN adsorbents and the Pb(II)–loaded ones were compared (Fig. 4*a*–*c*). The Figures revealed that the Pb(II)–loaded adsorbents spectra exhibited slight shifts and in most cases increased intensities in the spectra peaks in relation to the pristine GONH, GOSH and GOSN adsorbents. There were also appearances of few peaks for GONH (at ≈3062, 1511 and 1305 cm^{-1}), GOSH (at ≈3120, 2310 and 2056 cm^{-1}) and GOSN (at ≈3110, 1501 and 1316 cm^{-1}). These changes in peaks and new bands were ascribed to changes in vibrations due to the effects of the interactions of Pb(II) cations on the various functional groups (especially for the amine, thiol, carboxylate, and hydroxyl groups) at the adsorption sites of these adsorbents.

4. Conclusion

Mono- and dual-functionalized amino and thiol graphene oxide (GO) adsorbents were successfully synthesized, characterized and used for Pb(II) adsorption. The FTIR spectra confirmed that the APTES and MPTES moieties were attached to the GO sheets via the —OH functional group positions; the intensity of the —OH functional groups on the GO surface reduced in the new adsorbents and new peaks associated with the amine and thiol functional groups were evident. The X-ray diffraction spectra corroborated the FTIR spectra; unlike the GO, the spectra patterns of the functionalized adsorbents exhibited intense peak at $2\theta = 23^{\circ}$, while the GO $2\theta = 12^{\circ}$ peak was suppressed. According to the thermogravimetric analysis, the thermal stability of the GO material was lower than those of the new adsorbents by almost 70%. Thus, the new adsorbents were denser than GO.

The Pb(II) adsorption was spontaneous and weakly endothermic. The adsorption rate was high with up to 80% of total adsorption occurring within the initial 30 min of starting the experiment, but equilibrium was attained at 120 min, while optimum adsorption was observed at pH between 5 and 6. Isotherm models suggested that the adsorption mechanism involved electrostatic interactions between active functional groups and the Pb(II) cations, but the fit to a model (either Langmuir, Freundlich or Brouers–Sotolongo–fractal adsorption isotherm model) was dependent on the specific functional groups involved in the adsorbent. For instance, adsorption on the highly electrostatic functional groups having oxygen and nitrogen followed Langmuir model, while a combination of weak and strong functional groups (involving the above as well as sulphur groups) followed the Freundlich or more complex Brouers–Sotolongo–fractal adsorption isotherm model. Relative to adsorbents reported in literature, these

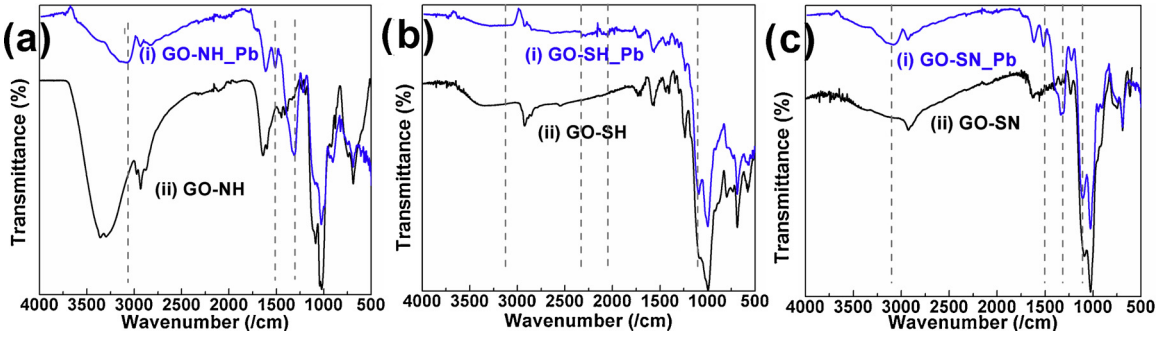

Fig. 4. Comparison of FTIR spectra before (ii) and after (i) adsorption of Pb(II) (a) GONH, (b) GOSH, and (c) GOSN.

adsorbents adsorption capacities points to their potential for treatment of Pb(II) in real wastewater.

Declaration of Competing Interest

The authors declare that they have no known competing financial interests or personal relationships that could have appeared to influence the work reported in this paper

Acknowledgments

We acknowledge the Department of Chemistry and Research Directorate, Vaal University of Technology, Vanderbiljpark, South Africa, and the SASOL Research grant (VAT Number: 4430113102).

Appendix A. Supplementary data

Supplementary material related to this article can be found, in the online version, at doi:https://doi.org/10.1016/j.jece.2019.103461.

References

[1] P.N. Diagboya, E.D. Dikio, Silica-based mesoporous materials; emerging designer adsorbents for aqueous pollutants removal and water treatment, Microporous Mesoporous Mater. 266C (2018) 252–267.
[2] P. Cruz-Tato, E.O. Ortiz-Quiles, K. Vega-Figueroa, L. Santiago-Martoral, M. Flynn, L.M. Díaz-Vázquez, E. Nicolau, Metalized Nanocellulose Composites as a Feasible Material for Membrane Supports: Design and Applications for Water Treatment, Environ. Sci. Technol. (2017).
[3] P.N. Diagboya, B.I. Olu-Owolabi, K.O. Adebowale, Synthesis of covalently bonded graphene oxide–iron magnetic nanoparticles and its kinetics of mercury removal, RSC Adv. 5 (2015) 2536–2542.
[4] B.I. Olu-Owolabi, A.H. Alabi, P.N. Diagboya, E.I. Unuabonah, R.-A. Düring, Adsorptive removal of 2,4,6-trichlorophenol in aqueous solution using calcined kaolinite-biomass composites, J. Environ. Manage. 192 (2017) 94–99.
[5] T.A. Kurniawan, M.E.T. Sillanpää, M. Sillanpää, Nanoadsorbents for Remediation of Aquatic Environment: Local and Practical Solutions for Global Water Pollution Problems, Crit. Rev. Environ. Sci. Technol. 42 (2012) 1233–1295.
[6] R.J.E. Leggiadro, Epidemics after natural disasters, Pediatr. Infect. Dis. J. 26 (2007) 552.
[7] ATSDR, Lead Toxicity: What Are U.S. Standards for Lead Levels, (2017) www.atsdr.cdc.gov/csem/csem.asp?=34&po=8.
[8] R.R. Pawar, M. Lalhmunsiama, J.-G. Kim, S.-M. Hong, S.Y. Sawant, S.M. Lee, Efficient removal of hazardous lead, cadmium, and arsenic from aqueous environment by iron oxide modified clay-activated carbon composite beads, Appl. Clay Sci. 162 (2018) 339–350.
[9] L. Aljerf, High-efficiency extraction of bromocresol purple dye and heavy metals as chromium from industrial effluent by adsorption onto a modified surface of zeolite: Kinetics and equilibrium study, J. Environ. Manage. 225 (2018) 120–132.
[10] P.N. Diagboya, E.D. Dikio, Dynamics of Mercury solid phase extraction using Barbula lambarenensis, Environ. Technol. Innov. 9 (2018) 275–284.
[11] B.I. Olu-Owolabi, P.N. Diagboya, E.I. Unuabonah, A.H. Alabi, R.-A. Düring, K.O. Adebowale, Fractal-like concepts for evaluation of toxic metals adsorption efficiency of feldspar-biomass composites, J. Clean. Prod. 171C (2018) 884–891.
[12] N. Daels, S. De Vrieze, I. Sampers, B. Decostere, P. Westbroek, A. Dumoulin, P. Dejans, K. De Clerck, S.W.H. Van Hulle, Potential of a functionalised nanofibre microfiltration membrane as an antibacterial water filter, Desalination 275 (2011) 285–290.
[13] S. Lin, R. Hsiao, R. Juang, Removal of soluble organics from water by a hybrid process of clay adsorption and membrane filtration, J. Hazard. Mater. 135 (2006) 134–140.
[14] T.A. Tabish, F.A. Memon, D.E. Gomez, D.W. Horsell, S. Zhang, A facile synthesis of porous graphene for efficient water and wastewater treatment, Sci. Rep. 8 (2018) 1817.
[15] C.N.R. Rao, A.K. Sood, K.S. Subrahmanyam, A. Govindaraj, Graphene: The New Two-Dimensional Nanomaterial, Angew. Chemie Int. Ed. 48 (2009) 7752–7777.
[16] D. Chen, H. Feng, J. Li, Graphene Oxide: Preparation, Functionalization, and Electrochemical Applications, Chem. Rev. 112 (2012) 6027–6053.
[17] V. Georgakilas, M. Otyepka, A.B. Bourlinos, V. Chandra, N. Kim, K.C. Kemp, P. Hobza, R. Zboril, K.S. Kim, Functionalization of Graphene: Covalent and Non-Covalent Approaches, Derivatives and Applications, Chem. Rev. 112 (2012) 6156–6214.
[18] P.N. Diagboya, B.I. Olu-Owolabi, D. Zhou, B.-H. Han, Graphene oxide–tripolyphosphate hybrid used as a potent sorbent for cationic dyes, Carbon 79 (2014) 174–182.
[19] M. Castelaín, G. Martínez, P. Merino, J.Á. Martín-Gago, J.L. Segura, G. Ellis, H.J. Salavagione, Graphene Functionalisation with a Conjugated Poly(fluorene) by Click Coupling: Striking Electronic Properties in Solution, Chem. Eur. J. 18 (2012) 4965–4973.
[20] S. Kabiri, D.N.H. Tran, M.A. Cole, D. Losic, Functionalized three-dimensional (3D) graphene composite for high efficiency removal of mercury, Environ. Sci.: Water Res. Technol. 2 (2016) 390–402.
[21] A.N. Ebelegi, N. Ayawei, D. Wankasi, E.D. Dikio, P.N. Diagboya, F.M. Mtunzi, Covalently bonded polyamidoamine functionalized silica used as a Pb(II) scavenger from aqueous solution, J. Environ. Chem. Eng. 7 (2019) 103214.
[22] X. An, T. Simmons, R. Shah, C. Wolfe, K.M. Lewis, M. Washington, S.K. Nayak, S. Talapatra, S. Kar, Stable Aqueous Dispersions of Noncovalently Functionalized Graphene from Graphite and their Multifunctional High-Performance Applications, Nano Lett. 10 (2010) 4295–4301.
[23] I.-Y. Jeon, H.-J. Choi, S.-M. Jung, J.-M. Seo, M.-J. Kim, L. Dai, J.-B. Baek, Large-Scale Production of Edge-Selectively Functionalized Graphene Nanoplatelets via Ball Milling and Their Use as Metal-Free Electrocatalysts for Oxygen Reduction Reaction, J. Am. Chem. Soc. 135 (2013) 1386–1393.
[24] A.K. Mishra, S. Ramaprabhu, Functionalized graphene sheets for arsenic removal and desalination of sea water, Desalination 282 (2011) 39–45.
[25] M.Z. Iqbal, M.S. Katsiotis, S.M. Alhassan, M.W. Liberatore, A.A. Abdala, Effect of solvent on the uncatalyzed synthesis of aminosilane-functionalized graphene, RSC Adv. 4 (2014) 6830–6839.
[26] S. Lagergren, Zur theorie der sogenannten adsorption gelöster stoffe, Kungliga Svenska Vetenskapsakademiens, Handlingar 24 (1898) 1–39.
[27] I. Langmuir, The constitution and fundamental properties of solids and liquids, J. Amer, Chem. Soc. 38 (1916) 2221–2295.
[28] H.M.F. Freundlich, Über die adsorption in lösungen, Zeitschrift für Physikalische Chemie 57A (1906) 385–470.
[29] P.N. Diagboya, B.I. Olu-Owolabi, K.O. Adebowale, Microscale scavenging of pentachlorophenol in water using amine and tripolyphosphate-grafted SBA-15 silica: Batch and modeling studies, J. Environ. Manage. 146 (2014) 42–49.
[30] R.A. Shawabkeh, Synthesis and characterization of activated carbo-aluminosilicate material from oil shale, Microporous Mesoporous Mater. 75 (2004) 107–114.
[31] X. Li, Z. Wang, Q. Li, J. Ma, M. Zhu, Preparation, characterization, and application of mesoporous silica-grafted graphene oxide for highly selective lead adsorption, Chem. Eng. J. 273 (2015) 630–637.
[32] Y.-F. Huang, P.-F. Wu, M.-Q. Zhang, W.-H. Ruan, E.P. Giannelis, Boron cross-linked graphene oxide/polyvinyl alcohol nanocomposite gel electrolyte for flexible solid-state electric double layer capacitor with high performance, Electrochim. Acta 132 (2014) 103–111.
[33] R.P. Mohubedu, P.N.E. Diagboya, C.Y. Abasi, E.D. Dikio, F. Mtunzi, Magnetic valorization of biomass and biochar of a typical plant nuisance for toxic metals contaminated water treatment, J. Clean. Prod. 209 (2019) 1016–1024.
[34] P.N. Diagboya, E.D. Dikio, Scavenging of aqueous toxic organic and inorganic cations using novel facile magneto-carbon black-clay composite adsorbent, J. Clean. Prod. 180 (2018) 71–80.
[35] S. Kabiri, D.N.H. Tran, M.A. Cole, D. Losic, Functionalized three-dimensional (3D) graphene composite for high efficiency removal of mercury, Environ. Sci. Water Res. Technol. 2 (2016) 390–402.
[36] H.O. Chukwuemeka-Okorie, P.N. Ekemezie, K.G. Akpomie, C.S. Olikagu, Calcined Corncob-Kaolinite Combo as New Sorbent for Sequestration of Toxic Metal Ions From Polluted Aqua Media and Desorption, Front. Chem. 6 (2018).
[37] I.A. Lawal, B. Moodley, Synthesis, characterisation and application of imidazolium based ionic liquid modified montmorillonite sorbents for the removal of amaranth dye, RSC Adv. 5 (2015) 61913–61924.
[38] C.Y. Abasi, P.N.E. Diagboya, E.D. Dikio, Layered double hydroxide of cobalt-zinc-aluminium intercalated with carbonate ion: preparation and Pb(II) ion removal capacity, Int. J. Environ. Stud. (2018) 1–15.
[39] S. Altenor, B. Carene, E. Emmanuel, J. Lambert, J.-J. Ehrhardt, S. Gaspard, Adsorption studies of methylene blue and phenol onto vetiver roots activated carbon prepared by chemical activation, J. Hazard. Mater. 165 (2009) 1029–1039.
[40] C. Xiong, S. Wang, W. Sun, Y. Li, Selective adsorption of Pb(II) from aqueous solution using nanosilica functionalized with diethanolamine: Equilibrium, kinetic and thermodynamic, Microchem. J. 146 (2019) 270–278.
[41] Z.-H. Huang, X. Zheng, W. Lv, M. Wang, Q.-H. Yang, F. Kang, Adsorption of Lead(II) Ions from Aqueous Solution on Low-Temperature Exfoliated Graphene Nanosheets, Langmuir 27 (2011) 7558–7562.
[42] L. Fan, C. Luo, M. Sun, X. Li, H. Qiu, Highly selective adsorption of lead ions by water-dispersible magnetic chitosan/graphene oxide composites, Colloids Surf. B Biointerfaces 103 (2013) 523–529.
[43] Z. Han, Z. Tang, S. Shen, B. Zhao, G. Zheng, J. Yang, Strengthening of Graphene Aerogels with Tunable Density and High Adsorption Capacity towards Pb2+, Sci. Rep. 4 (2014) 5025.
[44] Y.Q. He, N.N. Zhang, X.D. Wang, Adsorption of graphene oxide/chitosan porous materials for metal ions, Chinese Chem. Lett. 22 (2011) 859–862.
[45] L. Hao, H. Song, L. Zhang, X. Wan, Y. Tang, Y. Lv, SiO2/graphene composite for highly selective adsorption of Pb(II) ion, J. Colloid Interface Sci. 369 (2012) 381–387.
[46] Y. Zhang, L. Yan, W. Xu, X. Guo, L. Cui, L. Gao, Q. Wei, B. Du, Adsorption of Pb(II) and Hg(II) from aqueous solution using magnetic CoFe2O4-reduced graphene oxide, J. Mol. Liq. 191 (2014) 177–182.
[47] L. Cui, Y. Wang, L. Gao, L. Hu, L. Yan, Q. Wei, B. Du, EDTA functionalized magnetic graphene oxide for removal of Pb(II), Hg(II) and Cu(II) in water treatment: Adsorption mechanism and separation property, Chem. Eng. J. 281 (2015) 1–10.